

Contents

1	Simulation of Arbitrary Mixed-Mode Crack Growth Using an Energy-Based Approach	1
	B.R. Davis, P.A. Wawrzynek, and A.R. Ingraffea	
2	Experimental and Predicted Crack Paths for Al-2024-T351 Under Mixed-Mode I/II Fatigue	11
	E.E. Miller, M.A. Sutton, X. Deng, H. Watts, A.P. Reynolds, X. Ke, and H.W. Schreier	
3	On Numerical Evaluation of Mixed Mode Crack Propagation Coupling Mechanical and Thermal Loads in Wood Material	21
	Hassen Riahi, Rostand Moutou Pitti, Frédéric Dubois, and Eric Fournely	
4	Curvilinear Fatigue Crack Growth Under Out-of-Phase Loading Conditions	27
	Xiaomin Deng, Xiaodan Ke, Michael A. Sutton, Haywood S. Watts, and Hubert W. Schreier	
5	Fracture Surface Transition for Notched Bars in Torsion	35
	Alan T. Zehnder and Natasha Zella	
6	Mixed Mode Evaluation of Different Grinding Depths in FRPC Repairs	41
	T.S. Chawla and M.N. Cavalli	
7	Through Thickness Fracture Behavior of Transversely Graded Ti/TiB Material	51
	Behrad Koohbor, Silas Mallon, and Addis Kidane	
8	Coalescence and Growth of Two Semi-Elliptical Coplanar Cracks in API-5L Grade B Steel	57
	Abdallah Al Tamimi and Mohammad Modarres	
9	Measurement of Crack Tip Displacement Field in Desiccating Paste	67
	Tatsuya Arai and Kenichi Sakaue	
10	Characterization of Fracture Behavior of Multi-Walled Carbon Nanotube Reinforced Cement Paste Using Digital Image Correlation	73
	Nima Zohhadi, Behrad Koohbor, Fabio Matta, and Addis Kidane	
11	Characterization of Structural Scale Ductile Fracture of Aluminum Panels Using Digital Image Correlation	81
	K. Nahshon, W.A. Hoffman, and C.B. Ullagaddi	
12	Creep Damage Quantification and Post-fire Residual Strength of 5083 Aluminum Alloy	89
	Y. Chen, S.W. Case, and B.Y. Lattimer	
13	Nanoindentation Measurements on Rocks	99
	Priyavrat Shukla, Shantanu Taneja, Carl Sondergeld, and Chandra Rai	
14	Anelasticity in Al-Alloy Thin Films: A Micro-mechanical Analysis	107
	J.P.M. Hoefnagels, L.I.J.C. Bergers, and M.G.D. Geers	
15	Oxide Driven Strength Degradation on (111) Silicon	113
	Scott J. Grutzik and Alan T. Zehnder	

16	Impact of Speckle Pattern Parameters on DIC Strain Resolution Calculated from In-situ SEM Experiments	119
	Jennifer L.W. Carter, Michael D. Uchic, and Michael J. Mills	
17	Very High-Cycle Fatigue Resistance of Shot Peened High-Strength Aluminium Alloys: Role of Surface Morphology	127
	M. Benedetti, V. Fontanari, and M. Bandini	
18	Experimental Characterization of Semi-Rigidity of Standardized Lattice Beam Using the Grid Method	139
	Eric Fournely, Rostand Moutou Pitti, Evelyne Toussaint, and Michel Grediac	
19	Characterization of Martensitic Transformation Morphology in Wide Hysteresis Shape Memory Alloys ...	145
	Reginald F. Hamilton, Asheesh Lanba, and Osman Ozbulut	
20	Study of Phase Transformation Intermittency in S.M.A. Using the Grid Method	153
	Noemi Barrera, Xavier Balandraud, Michel Grédiac, Paolo Biscari, and Giovanni Zanzotto	
21	In-Situ X-Rays Diffraction and Multiscale Modeling of Shape Memory Alloys	157
	M.D. Fall, O. Hubert, K. Lavernhe-Taillard, and A. Maynadier	
22	Failure Mode Transition in Fiber Composite Fatigue	165
	Mohammad Rasheduzzaman and M.N. Cavalli	
23	Fracture Toughness and Impact Damage Resistance of Nanoreinforced Carbon/Epoxy Composites	173
	Joel S. Fenner and Isaac M. Daniel	
24	Fatigue Behavior of Glass-Bubbles Modified Adhesively Bonded Composite Joints	181
	Ermias G. Koricho, Anton Khomenko, and Mahmoodul Haq	
25	Experimental Observations of Dynamic Delamination in Curved [0] and [0/90] Composite Laminates	189
	I. Uyar, M.A. Arca, B. Gozluklu, and D. Coker	
26	Fatigue Failure of Polyethylene Electrofusion Joints Subject to Contamination	197
	Pedrom Tayefi, Stephen. B.M. Beck, and Rachel A. Tomlinson	
27	Creep Crack Growth in High-Temperature Impure Helium Environments	203
	D. Grierson, G. Cao, A. Glauddell, D. Kuettel, G. Fisher, P. Pezzi, P. Brooks, T. Allen, K. Sridharan, and W.C. Crone	
28	High-Frequency Resonance Phenomena in Materials Subjected to Mechanical Stress	211
	G. Lacidogna, B. Montrucchio, O. Borla, and A. Carpinteri	
29	Electromagnetic Emission as Failure Precursor Phenomenon for Seismic Activity Monitoring	221
	O. Borla, G. Lacidogna, E. Di Battista, G. Niccolini, and A. Carpinteri	
30	Wireless Acoustic Emission Monitoring of Structural Behavior	231
	A. Manuello, G. Lacidogna, G. Niccolini, and A. Carpinteri	
31	Acoustic Emission Monitoring of Rock Specimens During Fatigue Tests	239
	L. Zhou, A. Manuello, G. Lacidogna, R. Sesana, and A. Carpinteri	
32	Hybrid thermography and acoustic emission testing of fatigue crack propagation in Aluminum Samples ...	247
	C. Barile, C. Casavola, G. Pappalettera, and C. Pappalettere	

Chapter 1

Simulation of Arbitrary Mixed-Mode Crack Growth Using an Energy-Based Approach

B.R. Davis, P.A. Wawrzynek, and A.R. Ingraffea

Abstract A finite-element-based simulation technique is being developed to predict 3-D, arbitrary, non-planar evolution of mixed-mode crack growth. The approach combines a geometrically explicit crack front re-meshing scheme, and an energy-based growth formulation to predict extension magnitudes along the crack front. The technique also leverages a new 3-D mixed-mode energy release rate decomposition using the virtual crack extension (VCE) method. The energy-based crack growth formulation, previously implemented for planar crack growth, is extended to non-planar growth situations by employing a basis-function approach to describe crack front extensions. Rather than determining point-by-point extensions, calculating a governing function alleviates numerical influences on the crack growth predictions. The simulation technique seeks to mitigate computationally biased crack growth, as found in prescribed and mesh dependent methods, for example.

Keywords Crack growth • Energy release rate • Mixed-mode • Virtual crack extension • Finite-element analysis

1.1 Introduction

Many finite-element-based techniques have been developed to simulate 3-D arbitrary crack growth in structural components. Crack growth problems become inherently more difficult when complex loadings induce mixed-mode behavior. The resulting crack front evolution could become curved and tortuous. Utilizing a fracture mechanics approach to predict such complicated crack shape advances requires three main components: (1) crack representation, (2) fracture parameter calculations, and (3) crack extension application.

Currently, the prominent techniques for simulating 3-D, mixed-mode, arbitrary crack growth include the extended finite element method (XFEM) [1–3], cohesive zone elements [4, 5], and explicit crack front re-meshing schemes [6–9]. Each approach has been well developed throughout the literature, but as articulated in [10], suffer from some form of computational bias or require input on the expected crack evolution. For example, cohesive zone element approaches predict crack paths that are governed by the element locations, shapes, sizes and orientations. In some cases, finite element meshes are designed to adhere to the expected growth pattern, contradicting the notion of arbitrary crack evolution by linking a numerical artifact (the finite element mesh) with a physical phenomenon (crack growth). Alternatively, XFEM and re-meshing schemes often rely on user-prescribed growth increments to advance the front.

The unique crack growth simulation technique developed in [10] utilizes a new energy-based formulation that allows for the direct calculation of point-by-point crack front extensions. The formulation is derived from an energy expansion that depends on the first order variation of the energy release rate. The variation of energy release rate, made readily available via the virtual crack extension (VCE) method, acts as an influence function relating changes in energy from load increments to changes in geometry along the crack front. This term provides a mechanics-based approach to extract explicit crack extensions, avoiding the need to supply user-prescribed magnitudes of advance. The technique also employs a geometrically explicit crack representation that is continually updated through re-meshing schemes. As a result, mesh biased growth

B.R. Davis (✉) • P.A. Wawrzynek • A.R. Ingraffea
School of Civil and Environmental Engineering, Cornell University, 638 Rhodes Hall, Ithaca, NY 14853, USA
e-mail: brd46@cornell.edu

is reduced, allowing for the crack front to evolve arbitrarily. This form of crack representation is not a limitation of the technique, but deemed more practical for development purposes. The energy-based formulation can certainly be used with XFEM crack representations, for example.

The implementation of the simulation technique described in [10] is limited to mode I, planar crack growth conditions. It is the objective of the current work to extend the technique to simulate mixed-mode and non-planar, 3-D crack front evolution. To generalize the approach, an updated toolset is required. The commercial FRANC3D fracture analysis software [11] is used to represent and re-mesh the evolving non-planar crack front geometries. A new 3-D, mixed-mode VCE implementation (submitted and under review for publication) is developed to calculate the necessary energy release rates along the crack front. Finally, in conjunction with a trajectory criterion, a new basis-function approach to calculate extensions along an arbitrary front is constructed. The basis-function approach seeks to address sensitivity challenges associated with using a local, point-by-point approach for non-planar growth predictions. The focus of this proceeding will demonstrate the current status of the toolset development.

The next section will provide background and a description of the new 3-D, mixed-mode VCE implementation. Note that the full formulation and derivation of the mixed-mode VCE method will be available in an upcoming publication. Two examples are presented to verify the VCE mixed-mode energy release rate calculations. The following section will introduce the crack growth formulation, and its augmentation with the new basis-function methodology.

1.2 The Mixed-Mode Virtual Crack Extension Method

The VCE method for calculating energy release rates (also known as the stiffness derivative method) was first introduced by Dixon and Pook [12], and Watwood [13], and further developed by Hellen [14] and Parks [15]. Early VCE calculations utilized finite perturbations of meshes to approximate the required stiffness derivatives. This finite difference approach often introduced geometric approximation and numerical truncation errors. Using variational principle theories, a direct integral approach simplified the VCE method and improved accuracy and efficiency by eliminating the need for finite perturbations [16, 17]. The advent of the variational approach also allowed for the calculation of higher-order derivatives of energy release rate, the salient feature of the current method. Hwang et al. [18] generalized the variational formulations for planar 3-D cracks. A symmetric/anti-symmetric approach to decompose energy release rates, first demonstrated for a 2-D VCE method by Ishikawa [19] and later extended to 3-D equivalent domain J-integrals by [20–22], is used in the new 3-D VCE implementation.

1.2.1 Virtual Crack Extension Formulation

Following the formulation from [18], the VCE method is derived from the expression for the potential energy, Π , of a finite element system:

$$\Pi = \frac{1}{2} u^T K u - u^T f, \quad (1.1)$$

where u , K , and f are the displacement vector, the stiffness matrix, and the applied force vector, respectively.

The energy release rate, G , at crack-front position i is defined as the negative variation of the potential energy with respect to a virtual, incremental, crack-front extension, δa , in the normal direction of the front at that position:

$$G_i \equiv -\frac{\delta \Pi}{\delta A_i} = -\frac{\delta \Pi}{\delta a_i \ell_i}. \quad (1.2)$$

In the 3-D sense, the virtual extension has an associated area, δA_i , comprised of a virtual extension, δa_i , and an effective width, ℓ_i . Applying the variation to the finite element expression for potential energy leads to the following form of the energy release rate:

$$G_i = -\frac{1}{\ell_i} \left(\frac{1}{2} u^T \frac{\delta K}{\delta a_i} u - u^T \frac{\delta f}{\delta a_i} \right). \quad (1.3)$$

For simplicity in the current implementation, it is assumed that applied forces, f , are not influenced by the virtual incremental extension, and therefore the variational force term, $\frac{\delta f}{\delta a_i}$, is zero. The simplification reduces Eq. 1.3 to:

$$G_i = -\frac{1}{\ell_i} \left(\frac{1}{2} u^T \frac{\delta K}{\delta a_i} u \right). \quad (1.4)$$

Note, if the virtual extensions alter the nature of the applied load (e.g. with crack-face pressures, thermal, and body-force loadings), the effect must be accounted for with the variational force term, $\frac{\delta f}{\delta a_i}$, and included throughout the formulation.

The expression for the first-order variation of the energy release rate with respect to incremental crack extension, δa_j , follows from Eq. 1.4:

$$\frac{\delta G_i}{\delta a_j} = -\frac{1}{\ell_i} \left(u^T \frac{\delta K}{\delta a_i} \frac{\delta u}{\delta a_j} + \frac{1}{2} u^T \frac{\delta^2 K}{\delta a_i \delta a_j} u \right). \quad (1.5)$$

Note that Eqs. 1.4 and 1.5 represent the total global formulations of the VCE expressions for the energy release rate and rate of energy release rate. The integration and calculations are performed in a global coordinate system.

1.2.2 3-D Mixed-Mode Virtual Crack Extension Formulation

From Eq. 1.4, the energy release rate is composed of the stiffness derivative and nodal displacements. The stiffness derivative is fracture-mode invariant, leaving the displacements near the crack front to be decomposed into mode I, II, and III components. Using a local crack front coordinate system for each position along the front and the symmetric/anti-symmetric field decomposition found in [20], the local displacement modal contributions are determined such that:

$$u = u_I + u_{II} + u_{III}. \quad (1.6)$$

The decomposed displacements from Eq. 1.6 are substituted into Eq. 1.4, yielding the following expression for total energy release rate at position i :

$$G_i = -\frac{1}{\ell_i} \left[\frac{1}{2} (u_I + u_{II} + u_{III})^T \frac{\delta K}{\delta a_{iL}} (u_I + u_{II} + u_{III}) \right]. \quad (1.7)$$

Note that the stiffness derivative is also calculated in the local crack-front coordinate system to maintain consistency, and is denoted by subscript L . Expanding Eq. 1.7 leads to the separation of the decomposed energy release rate modes:

$$G_i = -\frac{1}{\ell_i} \left[\begin{aligned} & \left(\frac{1}{2} u_I^T \frac{\delta K}{\delta a_{iL}} u_I \right) + \left(\frac{1}{2} u_{II}^T \frac{\delta K}{\delta a_{iL}} u_{II} \right) + \left(\frac{1}{2} u_{III}^T \frac{\delta K}{\delta a_{iL}} u_{III} \right) \\ & + \left(u_I^T \frac{\delta K}{\delta a_{iL}} u_{II} \right) + \left(u_{II}^T \frac{\delta K}{\delta a_{iL}} u_{III} \right) + \left(\frac{1}{2} u_{III}^T \frac{\delta K}{\delta a_{iL}} u_I \right) \end{aligned} \right]. \quad (1.8)$$

Extending from Ishikawa's 2-D VCE mode decomposition [19], the mode I and II energy release rates are as follows:

$$G_{Ii} = -\frac{1}{\ell_i} \left(\frac{1}{2} u_I^T \frac{\delta K}{\delta a_{iL}} u_I \right), \quad (1.9)$$

$$G_{IIi} = -\frac{1}{\ell_i} \left(\frac{1}{2} u_{II}^T \frac{\delta K}{\delta a_{iL}} u_{II} \right). \quad (1.10)$$

The unique contribution of the current implementation is the inclusion of the mode III energy release rate distribution along the crack front. The remaining terms in Eq. 1.8, excluding Eqs. 1.9 and 1.10, comprise a pure mode III component, $\frac{1}{2}u_{III}^T \frac{\delta K}{\delta a_i L} u_{III}$, and three modal-interaction coupling terms. Understanding the influence of the coupling-mode terms is critical in determining their respective contributions to the 3-D mixed-mode energy release rates. Consider the following coupling mode terms from Eq. 1.8:

$$G_{I/II_i} = -\frac{1}{\ell_i} \left(u_I^T \frac{\delta K}{\delta a_i L} u_{II} \right), \quad (1.11)$$

$$G_{II/III_i} = -\frac{1}{\ell_i} \left(u_{II}^T \frac{\delta K}{\delta a_i L} u_{III} \right), \quad (1.12)$$

$$G_{III/I_i} = -\frac{1}{\ell_i} \left(u_{III}^T \frac{\delta K}{\delta a_i L} u_I \right). \quad (1.13)$$

Using symmetric and anti-symmetric arguments, it can be shown and verified numerically that calculating the coupling terms in Eqs. 1.11 and 1.13 about a symmetric domain lead to a cancellation effect. The result is $G_{III/I} = G_{III/III} = 0$. However, Eq. 1.12 has an additive effect that results in $G_{III/III} \neq 0$. The only contributing non-zero components to $G_{III/III}$ are out-of-plane shear. Therefore, any addition to the total energy release rate from $G_{III/III}$ must be a factor of the out-of-plane mode III energy release rate:

$$G_{III_i} = -\frac{1}{\ell_i} \left(\frac{1}{2} u_{III}^T \frac{\delta K}{\delta a_i L} u_{III} \right) + G_{II/III_i}. \quad (1.14)$$

With the individual mixed-mode terms determined and the modal-interaction coupling terms accounted for, the VCE total energy release is successfully decomposed, satisfying the following summation:

$$G_i = G_{I_i} + G_{II_i} + G_{III_i}. \quad (1.15)$$

1.2.3 Numerical Examples

In this section two verification analyses are presented to demonstrate the accuracy of the new, 3-D, mixed-mode energy release rate implementation using the VCE method. The mixed-mode VCE results are compared with analytical and M-integral methods. Each model and crack front geometry is meshed using the FRANC3D software.

The first problem considered a 45°-inclined circular crack centrally embedded within a rectangular isotropic body, as shown in Fig. 1.1. The model geometry was appropriately sized to approximate crack behavior within an infinite body. Analytical expressions for the mixed-mode I/II/III stress intensity factors for an inclined penny crack under remote tension [23] are used as a reference solution.

The second numerical example is a half-penny-shaped surface crack in an isotropic cylindrical specimen [24, 25]. Figure 1.2 shows the global geometry and loading conditions that induce mode II/III behavior along the crack front. The local, in-plane geometry of the crack front is depicted in Fig. 1.2. The VCE energy release rate results are compared with M-integral calculations using the FRANC3D software.

Figures 1.3 and 1.4 display the mixed-mode and total energy release rate distributions calculated by the VCE implementation for each example. The results compare extremely well with the reference solutions. The average percent differences between the VCE and reference results are 0.11 % and 0.23 % for the inclined circular crack and the surface-cracked cylinder, respectively.

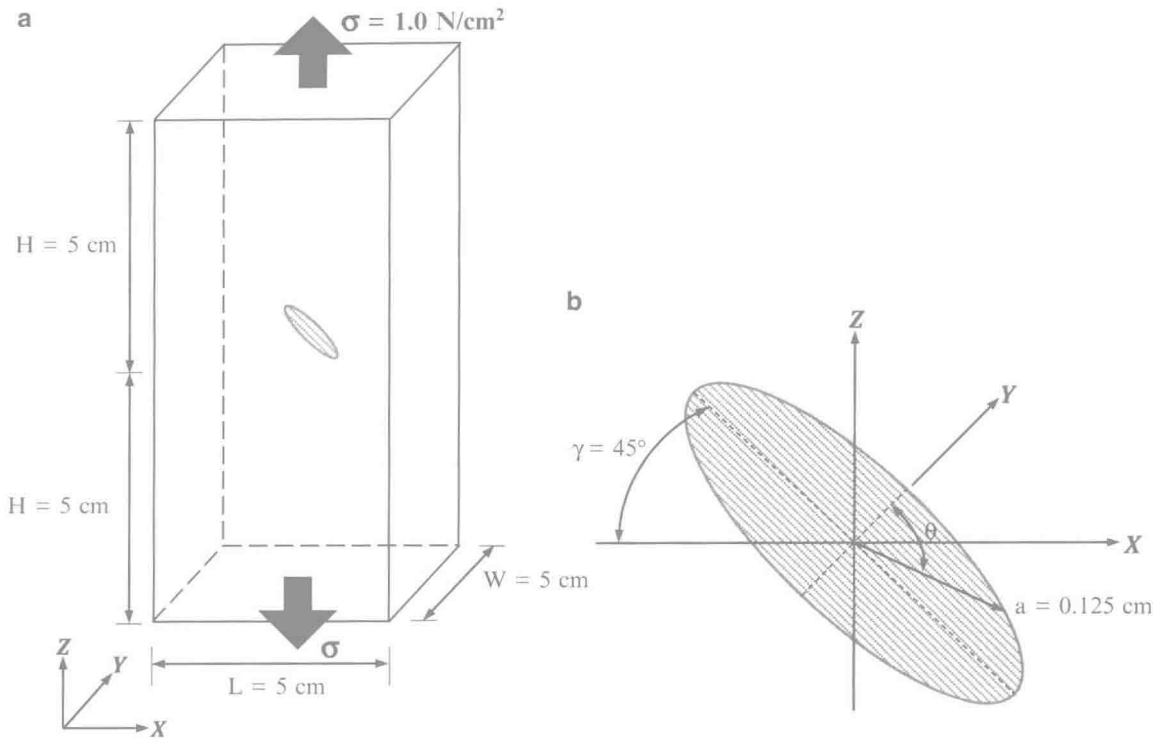


Fig. 1.1 Embedded inclined penny crack: (a) global geometry and loading conditions and (b) local crack-front geometry

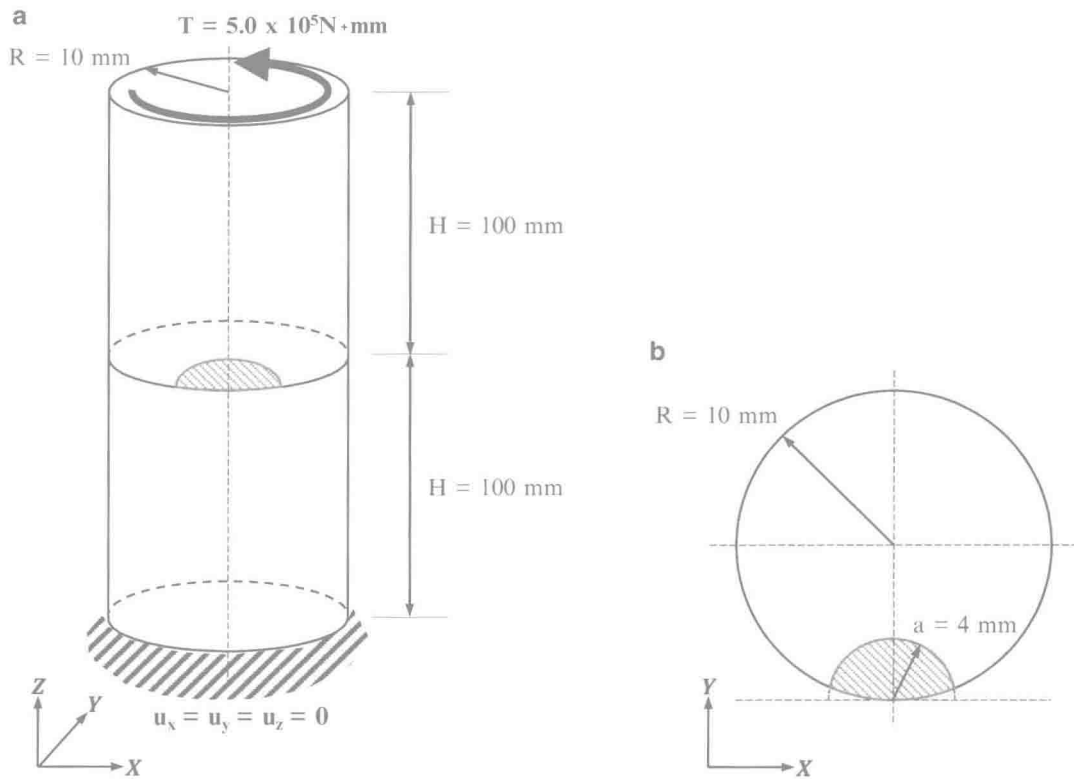


Fig. 1.2 Geometry and loading conditions for the penny-shaped surface crack in a cylindrical specimen: (a) global geometry and (b) local crack-plane geometry

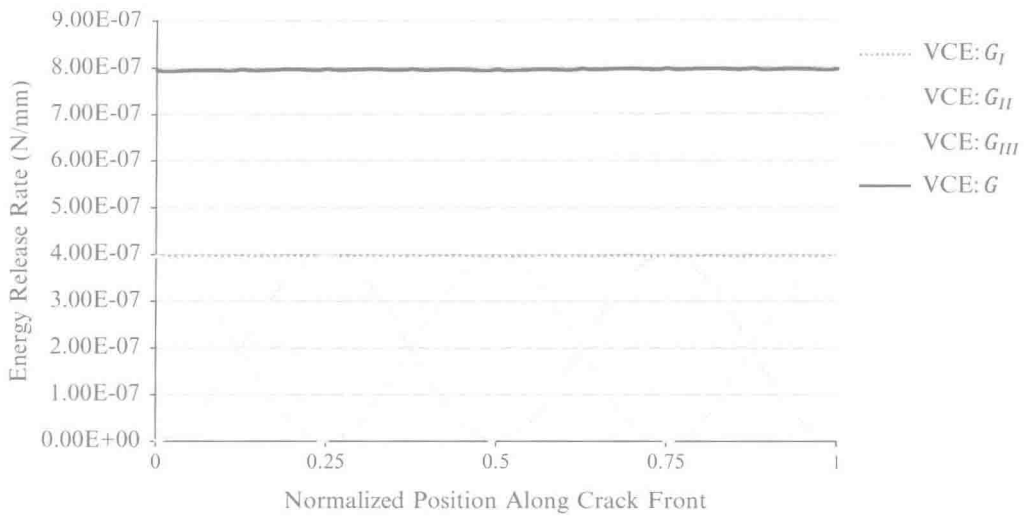
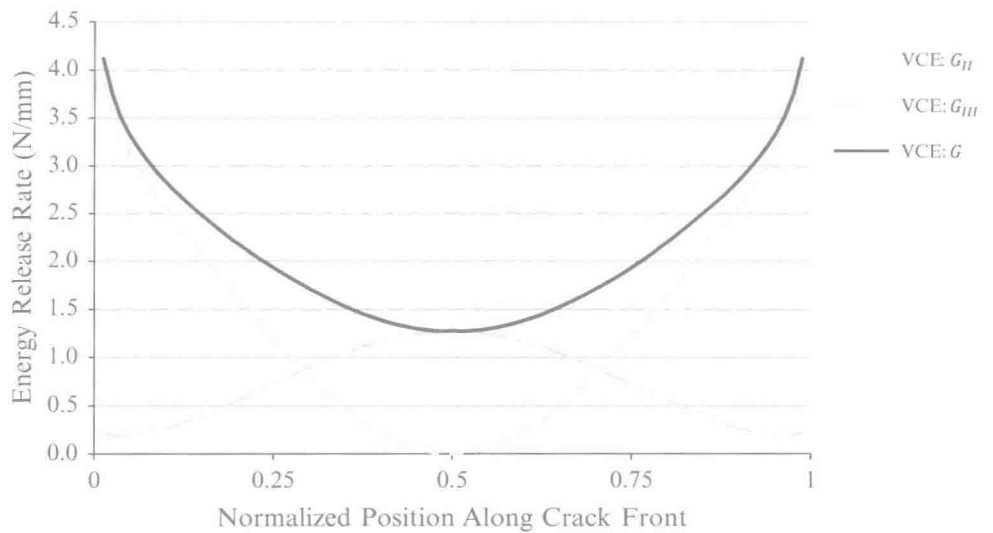


Fig. 1.3 Mixed-mode and total energy release rate distributions calculated by the VCE method for the inclined penny-crack specimen

Fig. 1.4 Mixed-mode and total energy release rate distributions calculated by the VCE method for the surface-cracked cylindrical specimen



1.3 Crack Growth Formulation

The prediction of mixed-mode, non-planar crack front extensions requires two features. The first is a crack trajectory or kinking approach to determine the angle of advance for a position along the front. The second is a crack growth formulation to calculate the magnitudes of advances.

1.3.1 Crack Trajectory Criterion

For this work, a maximum critical energy release rate criterion is employed to obtain the extension angles [26]. For each position on the front, a series of virtual extensions that sweep radially along the local crack front normal are applied and energy release rates calculated. From this distribution the angle associated with the maximum energy release rate is chosen as the local position's extension angle. Certainly, other mixed-mode trajectory and kinking criteria can be used, such as maximum tensile stress and maximum shear stress.

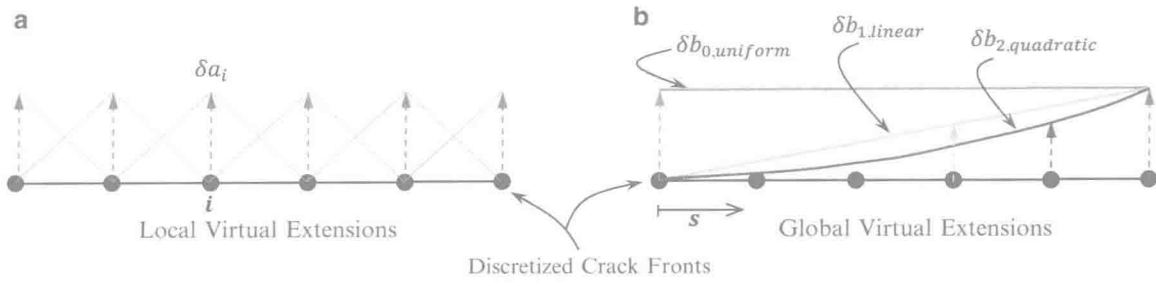


Fig. 1.5 Comparison between (a) local, point-by-point virtual crack extensions at position i , and (b) global basis-function virtual extensions along crack front length s

1.3.2 Basis-Function Growth Approach

The salient feature of this work is the modification of the crack growth formulation introduced in [10] to handle mixed-mode, non-planar growth situations. The planar growth formulation utilizes a balance equation extended from the first-order expansion of the energy release rate:

$$G_{ic} = G_i^0 + \frac{\delta G_i}{\delta P} \odot \Delta P_i + \frac{\delta G_i}{\delta a_j} \Delta a_j, \quad (1.16)$$

where G_{ic} is a critical energy release rate characterizing the material's resistance to crack growth; G_i^0 is the initial energy release rate prior to load increment ΔP_i ; $\frac{\delta G_i}{\delta P} \odot \Delta P_i$ represents the energy contribution due to the applied load increment; $\frac{\delta G_i}{\delta a_j} \Delta a_j$ represents the energy contribution due to crack shape change. The $\frac{\delta G_i}{\delta a_j}$ term is the aforementioned rate of energy release rate parameter obtained through the VCE method that acts as an influence function relating energy changes to crack shape changes. By comparing energy contributions at an initial load level and after an applied load increment, Eq. 1.16 can be rearranged to directly obtain Δa_j , the point-by-point crack front extensions. Note that the critical energy release rate used for material toughness can be substituted with a mixed-mode fracture criterion or effective critical value and is not limited to a single toughness parameter.

Two major issues were encountered when attempting to apply the formulation for planar cracks described in [10] to non-planar growth situations. First, numerical sensitivities associated with the VCE calculations and the complicated front geometries were observed. These nominally insignificant undulations in energy release rate distributions along the front transpire through the growth formulation to create inconsistencies in the calculated crack front extension. These inconsistencies can accumulate and render the crack growth predictions nonsensical. Another concern is the accuracy of the VCE rate of energy release rate calculation. The suspect term within Eq. 1.5 is the variation of nodal displacements, $\frac{\delta u}{\delta a_j}$. The term, essentially, is obtained by applying a local virtual point perturbation at each position along the crack front and then obtaining a finite element solution. Similar to applying a nodal force in a standard finite element model, the local virtual point perturbation creates a region of high distortion near the perturbation.

To assuage both sources of error a new approach is applied to the VCE method. Rather than using local, point-by-point virtual extensions, δa_j , to calculate the rate of energy release rate, a basis-function approach is used. A set of linearly independent functions distributed along the crack front, δb_j , is used as virtual extensions. The expression for the rate of energy release rate now becomes:

$$\frac{\delta G_i}{\delta b_j} = -\frac{1}{\ell_i} \left(u^T \frac{\delta K}{\delta a_i} \frac{\delta u}{\delta b_j} + \frac{1}{2} u^T \frac{\delta^2 K}{\delta a_i \delta b_j} u \right). \quad (1.17)$$

The necessary calculations for each term are executed in a similar fashion to the standard local VCE approach. However, the second order virtual extensions are now globally applied across the crack front. Figure 1.5 shows a schematic demonstrating the difference between the local, point-by-point approach, and an example global, basis-function approach comprised of uniform, linear, and quadratic functions.

The augmented rate of energy release rate expression alters Eq. 1.16 so that the formulation calculates the coefficients of the basis functions that, when combined, represent a function for the predicted extensions along the crack front. The predicted extensions are then applied at the determined angle in the same manner described in the planar crack growth scheme.

The basis-function technique provides insulation against numerical noise by restricting the extension along the front to be smooth and continuous. The function characterizing the predicted growth mitigates the influence of the minor fluctuations in the energy release rate distributions on the individual front extensions. Additionally, by distributing the virtual extensions along the entire front, the point perturbation issue in the variation of nodal displacements is alleviated. This is analogous to applying a distributed force, i.e. a pressure, instead of nodal forces to avoid distortion in finite element results.

At this point no non-planar crack front evolution has been predicted using the basis-function approach. However, preliminary simulations have used the basis-function methodology to predict planar crack growth in a double cantilever beam specimen with applied displacement increments. The simulated uniform growth of the straight crack front compares well with analytical calculations and the local approach results from [10]. The predicted crack lengths have a relative difference of less than 1 %.

1.4 Conclusions

The presented work develops the toolset required for a new simulation technique to predict arbitrary mixed-mode crack growth. The technique relies on an explicit geometric representation of the crack through the meshing tools of FRANC3D. Fracture mechanics parameters of interest are calculated by a new 3-D mixed-mode VCE method. Finally, the energy-based crack growth formulation of [10] is modified through a novel basis-function approach to determine non-planar crack front extensions.

The development and implementation of the toolset is ongoing. Preliminary results show promise for mixed-mode and non-planar growth simulations. The VCE implementation is being extended to calculate energy release rates for anisotropic material systems, such as delaminations in composite laminates. The basis-function approach continues to be tested, and is being integrated within an incremental iterative crack growth simulation scheme for non-planar growth simulations.

Acknowledgements This work was funded by the NASA University Institutes Project under Grant NCC3-989, and the Cornell University Ross-Tetelman Fellowship in Civil and Environmental Engineering.

References

1. Areias PMA, Belytschko T (2005) Analysis of three-dimensional crack initiation and propagation using the extended finite element method. *Int J Numer Methods Eng* 63:760–788
2. Huang R, Sukumar N, Prévost J-H (2003) Modeling quasi-static crack growth with the extended finite element method. Part II: Numerical applications. *Int J Solids Struct* 40:7539–7552
3. Sukumar N, Chopp DL (2008) Three-dimensional non-planar crack growth by a coupled extended finite element and fast marching method. *Int J Numer Methods Eng* 76:727–748
4. Roy YA, Dodds RH (2001) Simulation of ductile crack growth in thin aluminum panels using 3-D surface cohesive elements. *Int J Fract* 110:21–45
5. Khoei AR, Moslemi H, Sharifi M (2012) Three-dimensional cohesive fracture modeling of non-planar crack growth using adaptive FE technique. *Int J Solids Struct* 49:2334–2348
6. Carter BJ, Wawrzynek PA, Ingraffea AR (2000) Automated 3-D crack growth simulation. *Int J Numer Methods Eng* 47:229–253
7. Moslemi H, Khoei AR (2009) 3D adaptive finite element modeling of non-planar curved crack growth using the weighted superconvergent patch recovery method. *Eng Fract Mech* 76:1703–1728
8. Gürses E, Miehe C (2009) A computational framework of three-dimensional configurational-force-driven brittle crack propagation. *Comput Methods Appl Mech Eng* 198:1413–1428
9. Maligno AR, Rajaratnam S, Leen SB, Williams EJ (2010) A three-dimensional (3D) numerical study of fatigue crack growth using remeshing techniques. *Eng Fract Mech* 77:94–111
10. Davis BR, Wawrzynek PA, Ingraffea AR (2014) 3-D simulation of arbitrary crack growth using an energy-based formulation—Part I: Planar growth. *Eng Fract Mech* 115:204–220
11. FRANC3D 6.0.5. Fracture Analysis Consultants, Inc., Ithaca, NY, USA (2013) www.francanalysis.com
12. Dixon J, Pook L (1969) Stress intensity factors calculated generally by the finite element technique. *Nature* 224:166–167
13. Watwood VB Jr (1969) The finite element method for prediction of crack behavior. *Nucl Eng Des* 11:323–332
14. Hellen TK (1975) On the method of virtual crack extensions. *Int J Numer Methods Eng* 9:187–207
15. Parks DM (1974) A stiffness derivative finite element technique for determination of crack tip stress intensity factors. *Int J Fract* 10:487–502
16. Haber RB, Koh HM (1985) Explicit expressions for energy release rates using virtual crack extensions. *Int J Numer Methods Eng* 21:301–315
17. Lin SC, Abel JF (1988) Variational approach for a new direct-integration form of the virtual crack extension method. *Int J Fract* 38:217–235
18. Hwang CG, Wawrzynek PA, Ingraffea AR (2001) On the virtual crack extension method for calculating the derivatives of energy release rates for a 3D planar crack of arbitrary shape under mode-I loading. *Eng Fract Mech* 68:925–947

19. Ishikawa H (1980) A finite element analysis of stress intensity factors for combined tensile and shear loading by only a virtual crack extension. *Int J Fract* 16:243–246
20. Nikishkov GP, Atluri SN (1987) Calculation of fracture mechanics parameters for an arbitrary three-dimensional crack, by the “equivalent domain integral” method. *Int J Numer Methods Eng* 24:1801–1821
21. Shivakumar KN, Raju IS (1992) An equivalent domain integral method for three-dimensional mixed-mode fracture problems. *Engineering* 42:935–959
22. Huber O, Nickel J, Kuhn G (1993) On the decomposition of the J-integral for 3D crack problems. *Int J Fract* 64:339–348
23. Kassir MK, Sih GC (1974) Three-dimensional crack problems, *Mech. Fract. II*. Noordhoff International Publishing, Leyden
24. Levan A, Royer J (1993) Part-circular surface cracks in round bars under tension, bending and twisting. *Int J Fract* 61:71–99
25. Ismail AE, Ariffin AK, Abdullah S, Ghazali MJ (2012) Stress intensity factors under combined tension and torsion loadings. *Indian J Eng Mater Sci* 19:5–16
26. Hussain MA, Pu SL, Underwood J (1974) Strain energy release rate for a crack under combined mode I and mode II. In: *Fracture analysis*. American Society for Testing and Materials, ASTM STP 560. pp 2–28

Chapter 2

Experimental and Predicted Crack Paths for Al-2024-T351 Under Mixed-Mode I/II Fatigue

E.E. Miller, M.A. Sutton, X. Deng, H. Watts, A.P. Reynolds, X. Ke, and H.W. Schreier

Abstract The aerospace industry has experience with a range of structural failures, oftentimes due to fatigue cracks in aircraft fuselage components that are exposed to relatively high stress levels during cyclic loading effects that lead to fatigue crack initiation at material defects and near stress concentrations. These aircraft components are under complex stress states. In this study, mixed mode I/II fatigue experiments and simulations are performed for an Arcan fixture and a 6.35 mm thick Al-2024-T351 specimen, a popular aerospace alloy. Experiments were performed for Arcan loading angles that gave rise to a range of Mode I/II crack tip conditions from $0 \leq \Delta K_{II}/\Delta K_I \leq \infty$. Measurements include the crack paths, loading cycles, and maximum and minimum loads for each loading angle. Simulations were performed using three-dimensional finite element analysis (3D-FEA) with 10-noded tetrahedral elements via the custom in-house FEA code, CRACK3D. While modeling the entire fixture-specimen geometry, a modified version of the virtual crack closure technique (VCCT) with automatic crack tip re-meshing and a maximum circumferential stress criterion was used to predict the direction of crack growth. Results indicate excellent agreement between experiments and simulations for the measured crack paths during the first several millimeters of crack extension.

Keywords Mixed mode • Fatigue • Arcan • Crack path • Modeling

2.1 Introduction

The aerospace industry has experience with a range of structural failures, oftentimes due to fatigue cracks in aircraft fuselage components that are exposed to relatively high stress levels during cyclic loading effects incurred during repeated take-off and landing events that lead to fatigue crack initiation at material defects and near stress concentrations. Numerous event over the last 30 years have been recorded where fatigue cracks in the fuselage have propagated to critical areas resulting the cabin opening up mid-flight and causing cabin depressurization along with numerous injuries and, in one case, death [1–3].

In fact, fatigue cracks are expected to form in the fuselage of modern airplanes due to repeated (a) pressurization and decompression of the cabin during every flight and (b) loading effects during take-off and landing. Thus, the propagation of cracks into critical joints continues to be an area of concern, especially since such propagation under complex stress states is not completely understood. Although procedures are currently in place to inspect and repair fatigue cracks, the ability to better predict how far a crack will propagate and in which direction it would grow when subjected to various loading conditions could save millions of dollars in premature inspection and repair, while also identifying the severity of an existing flaw in an aero-structure.

E.E. Miller (✉) • M.A. Sutton • X. Deng • H. Watts • A.P. Reynolds
Department of Mechanical Engineering, University of South Carolina, 300 Main St., Columbia, SC 29208, USA
e-mail: eileen.e.miller@boeing.com

X. Ke • H.W. Schreier
Correlated Solutions, Inc., 121 Dutchman Blvd, Columbia, SC 29063, USA

J. Carroll and S. Daly (eds.), *Fracture, Fatigue, Failure, and Damage Evolution, Volume 5: Proceedings of the 2014 Annual Conference on Experimental and Applied Mechanics*, Conference Proceedings of the Society for Experimental Mechanics Series, DOI 10.1007/978-3-319-06977-7_2, © The Society for Experimental Mechanics, Inc. 2015

试读结束：需要全本请在线购买：www.ertongbook.com